3

Hemodynamics Study Based on Near-Infrared Optical Assessment

Chia-Wei Sun and Ching-Cheng Chuang
National Yang-Ming University,
Taiwan R.O.C.

1. Introduction

Blood, the body fluid responsible for transport materials and waste products, is composed of cells and plasma. More than 99 percent of the cells in blood are erythrocytes, which carry oxygen from and carbon dioxide to the lungs. The cardiovascular system is responsible for proper blood circulation throughout the body, and the ability of oxygen delivery plays an important role for vital sign monitoring, especially for cardiovascular insufficiency assessment for critical patients with heart failure, septic shock, and cerebral ischemia. Currently, the bedside assessment of cardiovascular adequacy often involves invasive hemodynamic monitoring, and is limited to the measurement of vital signs, blood lactate and capillary refill. Recently, noninvasive evaluation of activation-related tissue oxygenation changes has become available with near-infrared spectroscopy (NIRS). Since the NIRS method can evaluate the spatial distribution of tissue oxygenation in real-time, it has been proposed as an effective tool to quantify changes of local oxygenation in muscle tissue. In order to avoid the use of an exogenous tracer, the analysis of the dynamic response to oxy-hemoglobin (HbO_2) and deoxy-hemoglobin (Hb) during a standardized vascular occlusion test has been proposed for characterizing local metabolic rate, i.e., to analyze the concomitant temporal response of NIRS signal with applied vascular occlusion. Also, the tissue oxygen saturation (StO_2) and total hemoglobin (tHb) changes can be assessed by use of NIRS technique as markers of oxygen consumption and cardiovascular reserve with resting and exercising test.

2. Fundamentals of NIRS and diffuse optical method

2.1 Optical properties of biological tissues

Light propagating in a turbid medium like tissue will be scattered and absorbed by the randomly densely distributed heterogeneities (or particles), which may be cells or large molecules. To describe the absorption, we usually define an absorption coefficient μ_a (in cm^{-1}). The absorption in tissues is due to natural chromophores such as the hemo-pigment of hemoglobin, myoglobin, and bilirubin, the cytochrome pigments of the respiratory chain in the mitochondria, and melanin pigment. For scattering, a scattering coefficient μ_s (in cm^{-1}) is defined. The scattering in tissues is due to discontinuities in refractive index on the microscopic level, such as the aqueous-lipid membrane interfaces surrounding and within

each cell or the collagen fibrils within the extracellular matrix. For all optical diagnostic techniques aiming at the identification of pathologic areas, knowledge of the optical properties of tissues is of basic importance for a proper choice of the operation wavelengths. Such a wavelength should maximize the difference between the lesion to be detected and the surrounding healthy tissues, or more generally between the chromophore of interest and any other endogenous or exogenous chromophores present in tissues. The behavior of μ_a as a function of wavelength shows the typical spectral features of the main tissue constituents: blood hemoglobin, lipids, and water (Fig. 1).

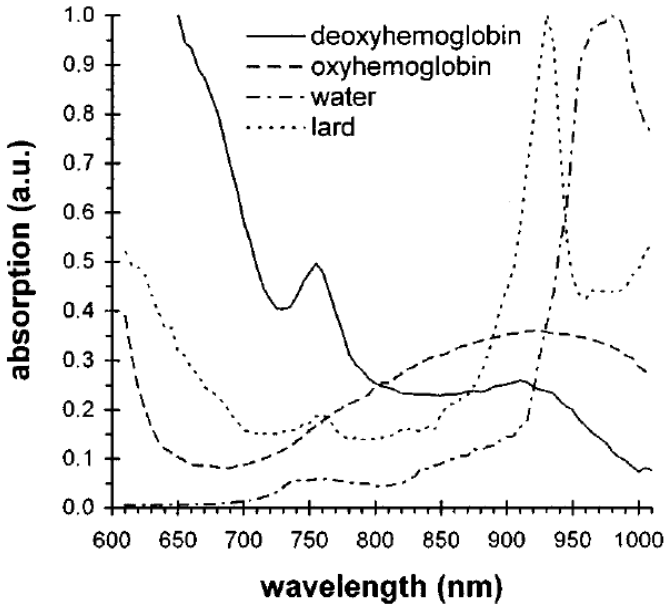

Fig. 1. Absorption spectra of the main tissue constituents: deoxy-hemoglobin (solid curve), oxyhemoglobin (dashed curve), water (dotted curve), and lard (dashed-dotted curve) [Cubeddu et al., 1999].

The transmitted photons can be divided into three types: ballistic (or coherent) photons, snake (or quasi-coherent) photons and diffuse (or multiply scattered) photons. Consider a short optical pulse incident upon a biological tissue. Figure 2 shows all the possibilities of photon scattering. We can see that the ballistic photons pass through the sample without any significant scattering. These photons will arrive at the detector earliest. The ballistic photons propagate in the direction of incoming beam, traverse the shortest path, and retain most information of the incident photons. However, the corresponding light intensity decreases quite rapidly with the propagation distance. Besides, some other photons experience certain forward scattering processes and are classified into the category of snake photon. Snake photons are scattered only slightly in the forward direction and transmit after the ballistic photons. Both ballistic and snake photons travel in the incident direction and arrive earlier than the multiple scattered diffuse photons. Those photons that experience many large-angle scattering processes have unpredicted transmitted angles and lose

information. Because of the long traveling path, diffuse photons are delayed in transmission. In some situations, a photon may experience many small-angle plus one large-angle scattering processes. Such a photon contributes to the group of backscattered photon. Because of the zero or weak random scattering, the ballistic, snake and backscattered photons carry more information for sample imaging compared with the diffuse photons.

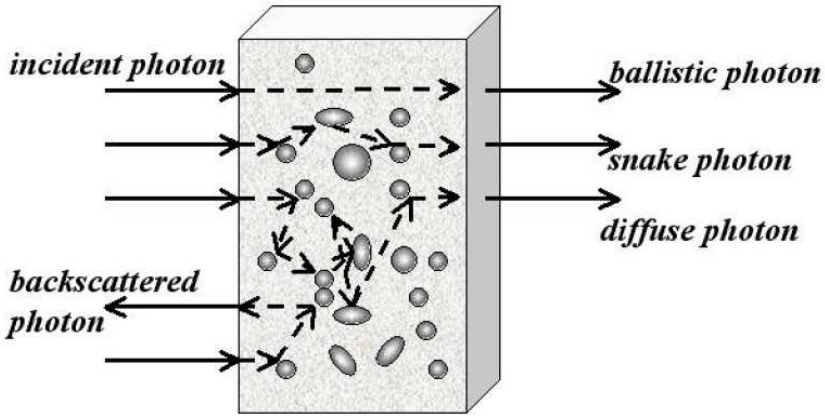

Fig. 2. Illustration of photon migration in a turbid medium.

When light encounters the biological tissue, there will be multiple effects of reflectance, absorption, and scattering due to the inhomogeneity. Even though, each tissue has its own characteristic optical absorption spectra, one can approximate the optical properties of tissues withot that of water, due to the facts of water is the major composition of human body, more than 70%. In blood, there are strong absorption in the visible range due to chromophores such as hemoglobin and bilirubin. Therefore, the absorption is dominated by the blood in tissue. There are also other chromophores that absorb light in the specific spectral range, such as melanin and proteins.

2.2 Light-tissue interaction

Light-tissue interaction, which is the basis for optically probing structure and function at cellular and tissue levels as well for the light-activated photodynamic therapy of cancer and other diseases; benefits from a molecular understanding of cellular and tissue structures and functions. Light propagation in biological tissues is governed by both absorption and scattering processes.

Absorption is the extraction of energy from light by a molecular species. The absorption can be mediated by either a radiative or an irradiative process. Irradiative absorption converts light energy to thermal energy. Radiative absorption introduces flourecence emission of longer wavelengths. Therefore, the ability of light to penetrate tissues depends on how strongly the tissues absorb light. At the short-wavelength end of therapeutic window, the window is bound by the absorption of hemoglobin, in both its oxygenated and deoxygenated forms. The absorption of oxygenated hemoglobin increases approximately two orders of magnitude as the wavelength shortens in the around 600 nm.

Scattering occurs where there is a spatival variation in the refractive index, either continuous or abrupt (e.g., due to localized particles). Scattering events can be further classified into elastic and inelastic ones. In elastic scattering, incident and scattered photons are of the same frequency. Such examples are Mie scattering (e.g., scattering particle size comparable to incident wavelength) and Rayleigh scattering (e.g., scattering particle size is smaller than incident wavelength). In inelastic scattering, incident and scattered photons are of different frequencies. Such examples are Brillouin scattering (e.g., emitting acoustic photons) and Raman scattering (e.g., emitting light of longer wavelengths). The level of inelastic scattering is much weaker as compared with that of elastic scattering, and is therefore negligible in diffuse optical imaging and spectroscopy. In blood, the disk-shaped red cells are the strongest scatters. The erythrocyte disk is ~2 μm thick with a diameter of 7 to 9 μm. The scattering properties of blood are dependent on the hematocrit (volume fraction of red cells) and its degree of agglomeration.

2.3 Near-infrared spectroscopy

NIRS measures tissue absorbance of light at several wavelengths in the spectral region from 600-1000 nm (called therapeutic windows), in which light can penetrate up to several centimeters into biological tissues, enabling deep-tissue imaging and tomography. At shorter wavelengths, the absorption of major tissue chromophores is significantly higher. Conversely, at longer wavelengths, the absorption of water is significantly higher. In addition, absorbing chromophores within biological tissues include such molecular structures as hemoglobin, myoglobin, water, melanin, cytochrome oxidase, bilirubin and

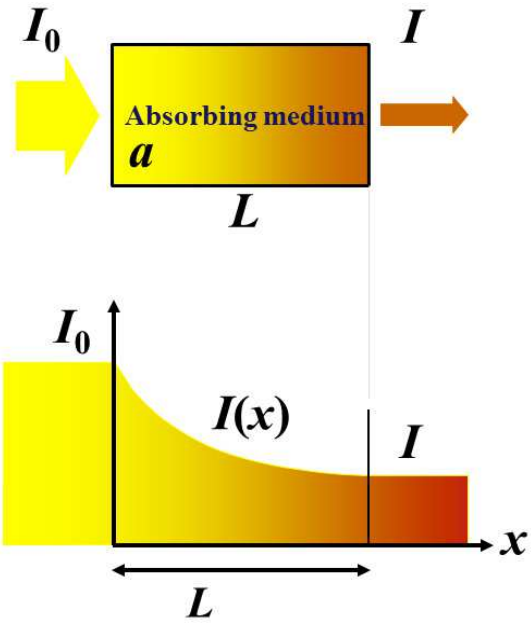

Fig. 3. Diagram of Beer-Lambert absorption of a beam of light as it travels through a slab of width L.

lipids. Contribution of each chromophore to tissue absorption spectrum can be calculated based on their concentrations in different tissue types. Thus enabling determination of concentration changes of oxygenated hemoglobin ([HbO_2]), deoxygenated hemoglobin ([Hb]), blood volume ([HbO_2]+[Hb]) and oxygenated cytochrome-oxidase. Absorption of light by tissue, causing light attenuation, depends on certain compounds that mentioned above. Light attenuation is measured in optical density (*OD*) and can be quantified using the Beer-Lambert's law. In other words, the Beer-Lambert's law relates the absorption of light to the properties of the material through which the light is traveling. The law states that there is a logarithmic dependence between the transmission *T*, of light through a substance and the product of the absorption coefficient of the substance *a*, and the distance the light travels through the material *L* (e.g., the path length). This situation is illustrated by Fig. 3.

Assume that particles may be described as having an absorption cross section (i.e., area), σ, perpendicular to the path of light through a solution, such that a photon of light is absorbed if it strikes the particle, and is transmitted if it does not. Define *x* as an axis parallel to the direction that photons of light are moving, and *dx* as the thickness of the slab which light is passing. We assume that *dx* is sufficiently small that one particle in the slab cannot obscure another particle in the slab when viewed along the *x* direction. The concentration of particles in the slab is represented by N' (the number density of absorbers). Expressing the number of photons absorbed by the slab as *dI*, and the total number of photons incident on the slab as *I*, the fraction of photons absorbed by the slab is given by

$$dI = -\sigma N' I dx \tag{1}$$

$$\frac{dI}{dx} = -\sigma N' I \tag{2}$$

Note that because there are fewer photons which pass through the slab than are incident on it, *dI* is actually negative (It is proportional in magnitude to the number of photons absorbed). The solution to this simple differential equation is obtained by integrating both sides to obtain *I* as a function of *x*

$$\ln(I) = -\sigma N' x + C \tag{3}$$

The difference of intensity for a slab of real thickness *L* is I_0 at $x = 0$, and *I* at $x = L$. Using the previous equation, the difference in intensity can be written as

$$\ln(I) - \ln(I_0) = (-\sigma N' L + C) - (-\sigma N' 0 + C) = -\sigma N' L \tag{4}$$

rearranging and exponentiating yields,

$$T = \frac{I}{I_0} = e^{-\sigma N' L} = e^{-\alpha' L} \tag{5}$$

This implies that the absorption is

$$A' = -\ln(T) = -\sigma N' L = -\alpha' L \tag{6}$$

$$A = OD = -\ln(T) = -\ln(\frac{I}{I_0}) = -\alpha LC \tag{7}$$

where C is the concentration of absorbing species in the material.

When light of a known wavelength is used to transilluminate a solution of a compound of unknown concentration *in vitro*, the absorption coefficient and thickness of solution traversed can be substituted in the Beer-Lambert equation to derive the concentration of the substance. Spectroscopy in this form has been used for many years in colorimetric analysis and, in certain circumstances, similar principles can be applied to biological tissue. Thus, in a biological tissue containing different absorbing compounds, the overall attenuation of the incident light at a given wavelength is calculated from the linear sum of the contributions of each compound. There are different absorbers to be considered for NIRS measurements contributing to total light attenuation such as HbO_2 and Hb. These absorbers show different absorption spectra, allowing spectroscopic separation using light of different wavelengths.

2.4 Diffuse optical tomography

The term diffuse optical tomography (DOT) refers to the optical imaging of biological tissue in the diffusive regime. DOT used the harmless near-infrared light that are advantageous because they are non-invasive, less expensive, nonradiative imaging, real-time measurement, compact implementation, long time monitoring, easy operation and the diffuse photon of NIR has a 1/e penetration depth on the order of 0.5 cm, near-infrared in the spectral window of 600-1000 nm wavelength can penetrate several centimeters into human breast tissue. Thus, far DOT has generated a lot of scientific interest and has been applied in various deep-tissue applications such as imaging of brain, breast, limb and joint. According to the type of operation, DOT can be classified into three modes as time domain, frequency domain and continuous wave (Fig. 4).

In all three modes, the reemitted light has the same general form as the source light since the system is linear and time-invariant. In the time domain operation, the optical properties of the tissue are inferred from the temporal point spread function (TPSF), i.e., the temporal response to an ultra-short pulse of light source. Thus, time domain DOT is a kind of "time gating" approach to increase the spatial resolution and it reveals rich depth information. The ballistic photons take the shortest path through the medium, arriving at the detector first. Then, strongly scattered photons (diffused light), arriving with increasing delay, presents a corresponding increase in light path length and transverse excursion uncertainty. In the frequency-domain mode, the source light intensity is amplitude-modulated sinusoidally at typically hundreds of MHz, and the reemitted light modulation has reduced modulation depth (AC amplitude/DC). In the DC mode, the source light is usually time-invariant, but it is sometimes modulated at low frequency (e.g., kHz) to improve the signal-to-noise ratio (SNR) or to encode the source. Such low-frequency modulation, however, does not attain the benefits of the frequency-domain mode. The time-domain and the frequency-domain modes are mathematically related via the Fourier transformation. If measured at many frequencies (including DC) in a sufficiently broad bandwidth, frequency-domain signals can be converted to the time domain using the inverse Fourier transformation. Therefore, the time-domain mode is mathematically equivalent to the combination of the frequency-domain and DC modes. Further, the DC mode is a zero-frequency special case of the frequency-domain mode.

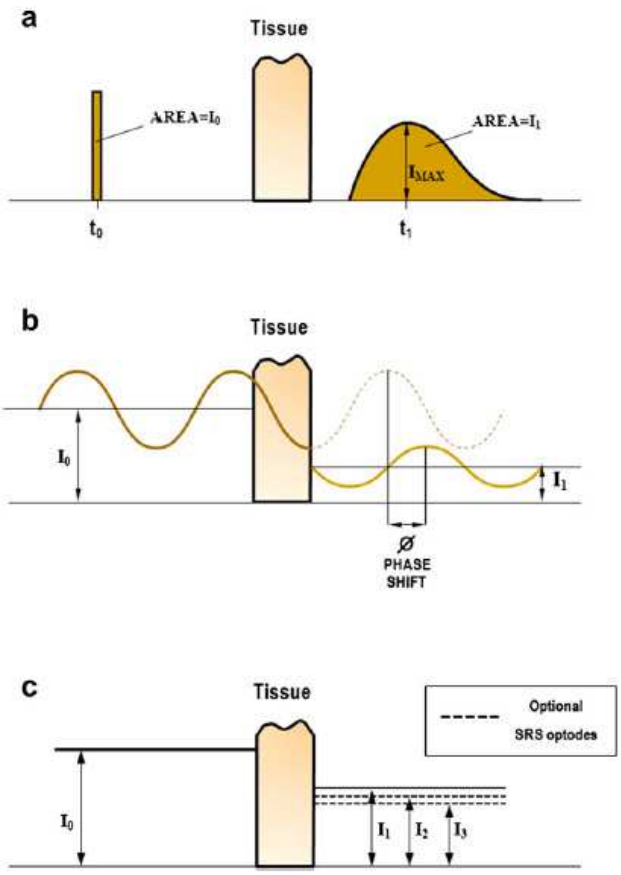

Fig. 4. Source excitation and signal detection for three types of diffuse optical systems. (a) Time domain, (b) Frequency domain, (c) Continuous wave [Pellicer et al., 2011].

DOT offers the capability to simultaneously quantify the tissue concentration of both HbO_2 and Hb. All DOT instrumentation should be designed with the following parameters:

- large dynamic range
- linearity
- stray light rejection
- crosstalk reduction
- long-term stability
- good temporal response

In a DOT system, sources and detectors are placed around the object to be imaged in various geometric configurations. Common geometric configurations, suited for different applications, fall into planar transmission, planar reflection, and cylindrical reemission. Most anatomical sites can be imaged in the planar reflection configuration. Generally, while one source illuminates the object, all detectors measure the reemitted light. This process is

repeated with each source to complete a measurement data set; subsequently, images are reconstructed by computer.

3. Monitoring of oxygen consumption and hemodynamic

Local blood flow (BF), expressed in *ml* of blood per 100 ml of tissue per minute, and oxygen consumption (OC), expressed in *μmol* of O_2 per 100 ml of tissue per minute, are relevant physiological parameters. Over the past decade, NIRS has been shown to be an effective tool for measuring local changes in tissue oxygenation and perfusion. NIRS measures tissue blood flow using different protocols such as the arterial occlusion test (AOT) and the venous occlusion test (VOT). These protocols are noninvasive and allow simultaneous measurements of local BF and OC in skeletal muscles. This technique has demonstrated a strong correlation with xenon and plethysmographic methods, both in resting and exercising subjects. *In situ* muscle oxygen consumption can be measured by NIRS during AOT (the pneumatic cuff is inflated to a pressure of about 240 mm Hg). The increase in Hb during AOT can be attributed to the conversion of HbO_2 into Hb. Although inducing ischemia through arterial occlusion provides additional information on local muscular metabolic energy, this process runs the risk of tissue necrosis in critical patients. Thus, a VOT (the pneumatic cuff is inflated to a pressure of about 50 mm Hg) was adopted to estimate the consumption of oxygen by muscles and blood flow using the same techniques of conventional venous plethysmography. Venous occlusion testing was performed using a controllable pneumatic tourniquet around the upper arm, causing an increase in the volume of blood in the forearm due to undisturbed forearm arterial inflow and interrupted venous outflow. Thus, changes in HbO_2, Hb, and total Hb (tHb) during venous occlusion were induced only through arterial inflow and the consumption of oxygen by tissue. The fundamental measurement associated with the DOSI system is the intensity of light after traveling through the tissue. The intensity of the light signals was measured and analyzed according to the modified Beer-Lambert law. The modified Beer-Lambert law is as follows:

$$OD = -\log(\frac{I}{I_0}) = \varepsilon CLB + G \tag{8}$$

where OD is the optical density. I_0 and I are the intensity of incident light and detected light, respectively. ε represents the extinction coefficient of the tissue; C is the concentration of the tissue. L represents the mean path length of detected photons. B is the path length factor set for the compensation of various effective path lengths of various wavelengths. G is defined as the geometric factor used to compensate the objective with different geometrical shapes. Typically, L, B and G are constants with monochromatic illumination in a turbid media with unchanging geometry. Changes in optical signaling were measured concomitantly with changes in the oxygenation of tissue. Then equation (8) can be rewritten as:

$$\Delta OD = OD_{Final} - OD_{Initial} = -\log(\frac{I_f}{I_i}) = \varepsilon \Delta CLB \tag{9}$$

where ΔOD is the change in optical density. OD_{Final} and $OD_{Initial}$ are detected optical density and the optical density of incident light. If and I_i are the measured intensities before and after the change in concentration; ΔC is the change in concentration. Changes in detected

light intensity were dominated by changes in the concentration of HbO_2 and Hb in the tissue. Therefore, the description can be treated as follows:

$$\Delta OD^{\lambda} = (\varepsilon_{HbO_2}^{\lambda} \cdot \Delta[HbO_2] + \varepsilon_{Hb}^{\lambda} \cdot \Delta[Hb]) B^{\lambda} L \tag{10}$$

$$\Delta[HbO_2] = \frac{\varepsilon_{Hb}^{\lambda_1} \cdot (\Delta OD^{\lambda_2} / B^{\lambda_2}) - \varepsilon_{Hb}^{\lambda_2} \cdot (\Delta OD^{\lambda_1} / B^{\lambda_1})}{(\varepsilon_{Hb}^{\lambda_1} \cdot \varepsilon_{HbO_2}^{\lambda_2} - \varepsilon_{Hb}^{\lambda_2} \cdot \varepsilon_{HbO_2}^{\lambda_1}) L} \tag{11}$$

$$\Delta[Hb] = \frac{\varepsilon_{HbO_2}^{\lambda_2} \cdot (\Delta OD^{\lambda_1} / B^{\lambda_1}) - \varepsilon_{HbO_2}^{\lambda_1} \cdot (\Delta OD^{\lambda_2} / B^{\lambda_2})}{(\varepsilon_{Hb}^{\lambda_1} \cdot \varepsilon_{HbO_2}^{\lambda_2} - \varepsilon_{Hb}^{\lambda_2} \cdot \varepsilon_{HbO_2}^{\lambda_1}) L} \tag{12}$$

$$B = \frac{1}{2}\sqrt{\frac{3\mu_s'}{\mu_a}}\left[1 - \frac{1}{(1 + L\sqrt{3\mu_s'\mu_a})}\right] \tag{13}$$

The oxygenation saturation StO_2 and the concentration of total hemoglobin can be calculated from concentrations of HbO_2 and Hb based on Eqs. (14) and (15):

$$StO_2 = \frac{\Delta[HbO_2]}{\Delta[HbO_2] + \Delta[Hb]} \tag{14}$$

$$tHb = \Delta[HbO_2] + \Delta[Hb] \tag{15}$$

Generally, temporally-applied low cuff pressures (50 mm Hg in our cases) occlude venous outflow while minimizing the obstruction of arterial inflow. An increase in deoxygenated

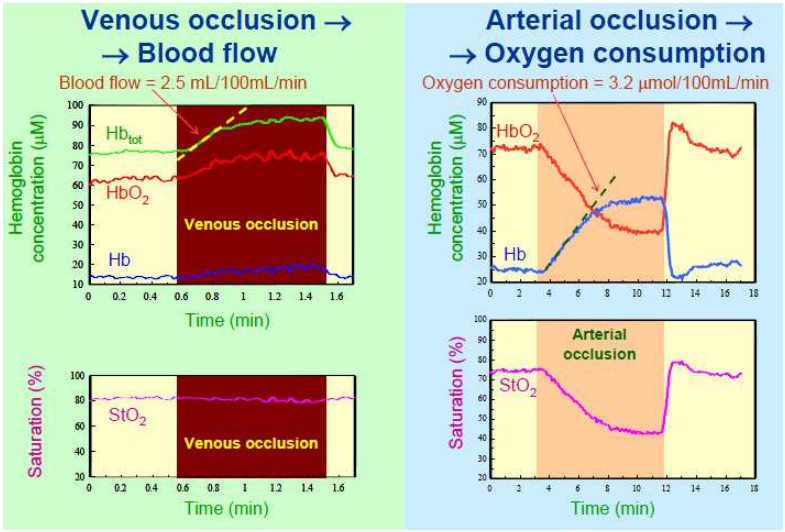

Fig. 5. Changes in forearm hemoglobin concentration and saturation induced by VOT (left) and AOT (right) in the upper arm [Sergio Fantini's Group, Department of Biomedical Engineering, Tufts University].

blood is then used to determine the level of oxygenation in muscle. Near-infrared spectroscopy assesses the level of oxygenation and the volume of blood in local tissue, and VOT has been shown to provide results in agreement with those obtained from traditional measurements employing plethysmography with calculations based on the Fick principle.

Figure 5 shows typical traces of hemoglobin concentration and saturation measured in the brachioradialis muscle (forearm) of a human subject during VOT and AOT. The main effect of the venous occlusion is to increase the hemoglobin concentration, as a result of blood accumulation. The tissue desaturation during arterial occlusion results from a rate of decrease of [HbO_2] that is equal to the rate of increase of [Hb] because the [tHb] remains constant during arterial occlusion. The initial rate of increase of [tHb] during VOT can be translated into a measurement of BF. The initial rate of increase of [Hb] during AOT can be translated into a measurement of the oxygen consumption.

4. The correlation between tissue oxygenation and erythrocytes elasticity

The change of tissue oxygenation resulted from several physiological conditions: cardiac output, pulmonary circulation, systemic circulation, oxygen consumption of tissue, and characterization of red blood cells (RBCs). Human erythrocytes have the shape of a biconcave disk (approximately 7 μm in diameter), which imparts a high surface-to-volume ratio so that oxygen and carbon dioxide can rapidly diffuse to and from the interior of the cell. Erythrocytes are highly deformable, which is essential for them to pass through small capillaries in microcirculation circuits. Furthermore, the deformability reveals the inherent property of erythrocytes that has been proved for differentiation between normal RBCs and malaria-infected RBCs. In this case, malaria-infected RBCs are manifested to be much less deformable, in comparison with normal RBCs. Optical tweezers have been utilized to quantify the deformability of erythrocytes with noninvasive trapping and stretching. Although the optical tweezers can be adopted for the probing of RBC mechanical properties that reveals the physiological states of erythrocyte, there is no direct evidence that shows the contribution of erythrocyte elasticity for blood-oxygen supplement in human circulation system. The correlation between erythrocyte elasticity and tissue oxygenation is investigated based on jumping optical tweezers and NIRS measurement. When the noninvasive monitoring the dynamic response to tissue oxygenation during an induced ischemia process by AOT could characterize local metabolic rate of muscle energy and tissue oxygenation recovery behavior with the assumption that tHb is constant. The AOT was utilized to estimate muscle oxygen consumption by applying the same technique as that used in conventional plethysmography. In the jumping optical tweezers system, the AC voltage is used to drive the diffracted beam that produced a 1-kHz square wave for the RBC stretching. The jumping distances are set from 3.8 μm to 5.9 μm in the experiments. In the Kelvin–Voigt viscoelastic solid model, the RBC can be treated as a spring model with elastic constant k and damping coefficient b. Thus, the values of erythrocyte elasticity and viscosity can be obtained from jumping tweezers probing.

Figure 6. shows the average difference of oxygenation temporal tracings between the two groups. Generally, both temporal profiles demonstrate the typical pattern that indicates the isolated increase in metabolic rate of oxygen based on a one-compartment model. The Hb rising is caused by oxygen consumption by arterial occlusion followed reactive hyperemia. The concentration of HbO_2 declines under the concomitant condition of oxygen supplement

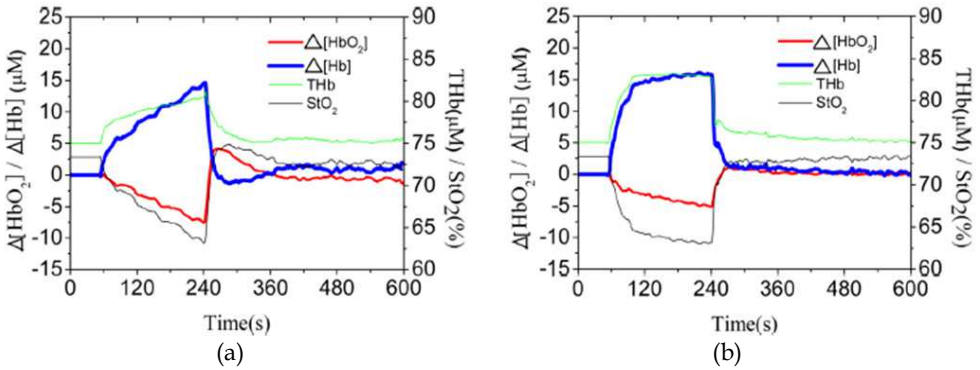

Fig. 6. Temporal tracings of tissue oxygen saturation (StO_2), total hemoglobin (THb), oxy-hemoglobin (HbO_2) and deoxy-hemoglobin (Hb) response to an AOT assessment: (a) the slower response of oxygenation dynamics, and (b) the faster response of oxygenation dynamics [Wu et al., 2011].

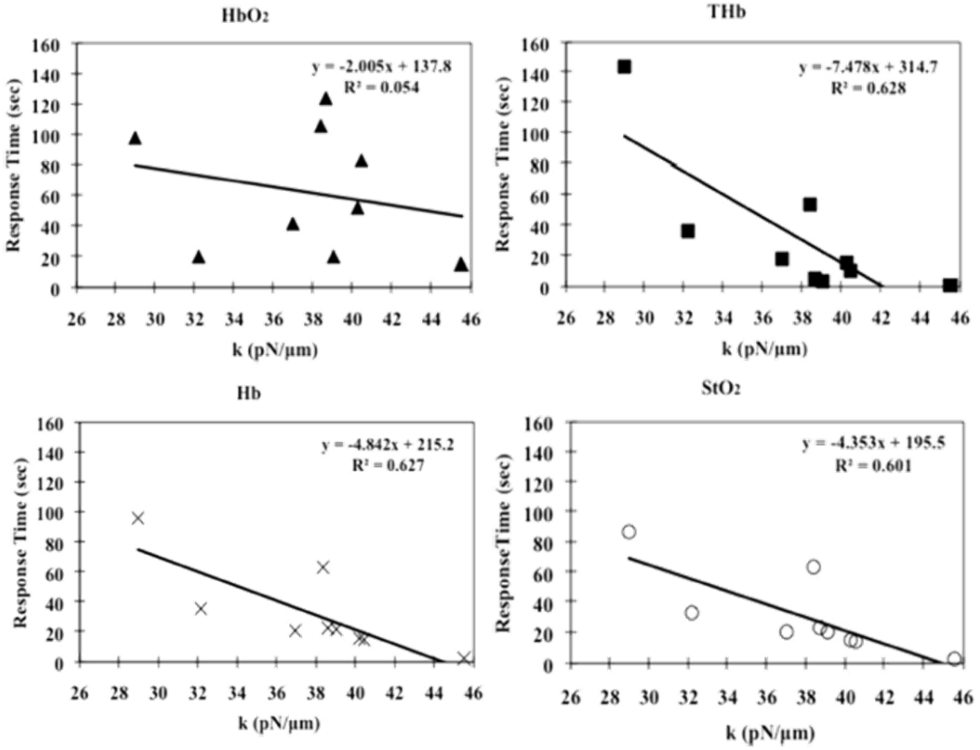

Fig. 7. The correlation between the response time of oxygenation signal and erythrocyte elasticity. The R^2 values for elastic constant versus response time of HbO_2, Hb, tHb and (d) StO_2 [Wu et al., 2011].

interrupted to the muscle. Group 1 is a slower change rate of oxygenation during AOT. Quantitatively, the increasing time of Hb concentration to 80% of the maximum value is more than 100 s in group 1. On the contrary, the dynamic oxygenation signals of AOT from group 2 respond faster than group 1.

The interpretation of the results from NIRS and optical tweezers is based on an assumption: the AOT-induced dynamic oxygenation signal is dependent on the related erythrocytes elasticity in vessels. The lower k implies higher deformability of RBC. During the application of high pressure on the extremity, the vessels were blocked for blood circulation. RBC with higher deformability may offer more oxygen supplement to muscle because of its higher passing ability in obstructed vessels. This phenomenon can be indicated from the tardier rising/falling of oxygenation tracings during AOT in group 1. The correlations are linearly fitted between the erythrocyte elastic constant and the response time of HbO_2, Hb, tHb, and StO_2 in Fig. 7. The response time is defined as the time spent while the oxygenation response reached the half-maximum value after arterial occlusion. The coefficient of determination R^2 (the square of the correlation coefficient) is than calculated for each case. Thus, the RBC elasticity is more strongly related to the Hb response than HbO_2, e.g. the change of Hb concentration dominates the correlation between erythrocyte elasticity and AOT-induced tissue oxygenation dynamics. Besides, similar evidence is also revealed in tHb and StO_2 plots. This result is reasonable because the tHb and StO_2 signals are both led from changes of Hb. The experimental results show a linear correlation between the oxygenation signal caused by AOT and the elasticity of erythrocytes.

5. The clinical applications of the near-infrared oxygenation monitoring

5.1 Cerebral oxygenation

The high sensitivity of NIRS to changes in the tissue hemoglobin concentration (changes as small as 0.05-0.10 μM in tissues can be detected) affords the optical detection of small cerebral hemodynamic fluctuations. NIRS is a promising non-invasive brain imaging technique with a high sampling rate, precise and localized spatial resolution. The NIRS technique provides information about the slow signal (i.e., hemoglobin response) and fast signal (i.e., neuronal activation) of neuron-vascular coupling (Fig. 8). The slow signal occurs in the range of seconds after the onset of the stimulation and reflects mainly changes in light absorption property in brain. On the contrary, the fast signal is believed to result from light scatter changes that are associated with ion currents across the neural membrane, which appear in the range of milliseconds after stimulation.

Neurovascular coupling is the generic term for changes in cerebral metabolic rate of oxygen ($CMRO_2$), cerebral blood flow (CBF), and cerebral blood volume (CBV) related to brain activity. NIRS detects changes in [HbO_2] and [Hb] and therefore total hemoglobin concentration [tHb], which corresponds to CBV. CBF and $CMRO_2$ also affect the [HbO_2] and [Hb] traces. Assuming a one-compartment model (Fig. 9), an isolated change in CBF will have the depicted effect on the [HbO_2] and [Hb]. The increase in CBF will lead to an increase in [HbO_2] and a decrease in [Hb] because more oxygenated than deoxygenated blood will fill the compartment. This effect is often described as the washout effect. Note that the changes are completely symmetrical. This NIRS method permitted several benefits as non-invasive, less expensive, non-ionizing radiation imaging, real-time measurement, compact implementation, long time monitoring and easy operation with high time resolution and

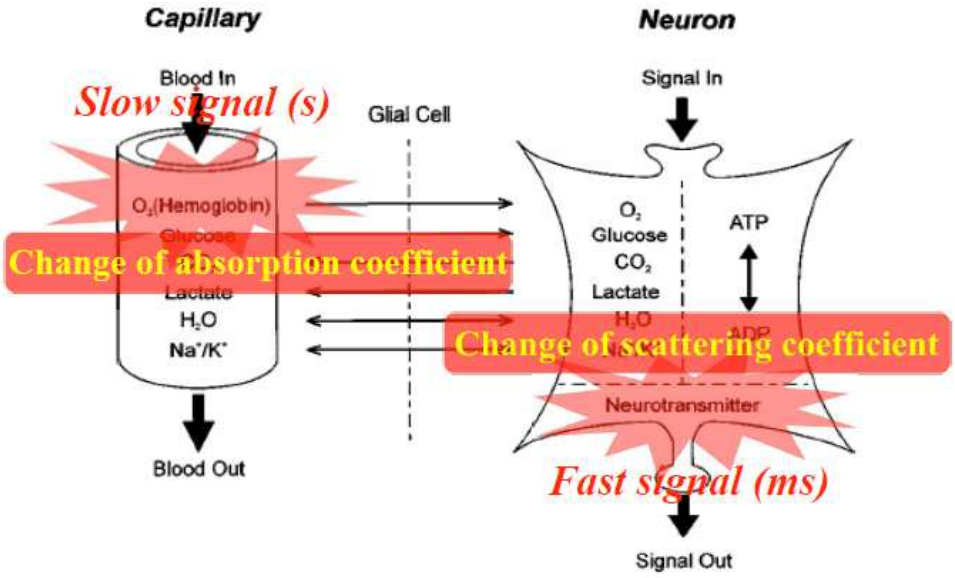

Fig. 8. Neuron-vascular coupling

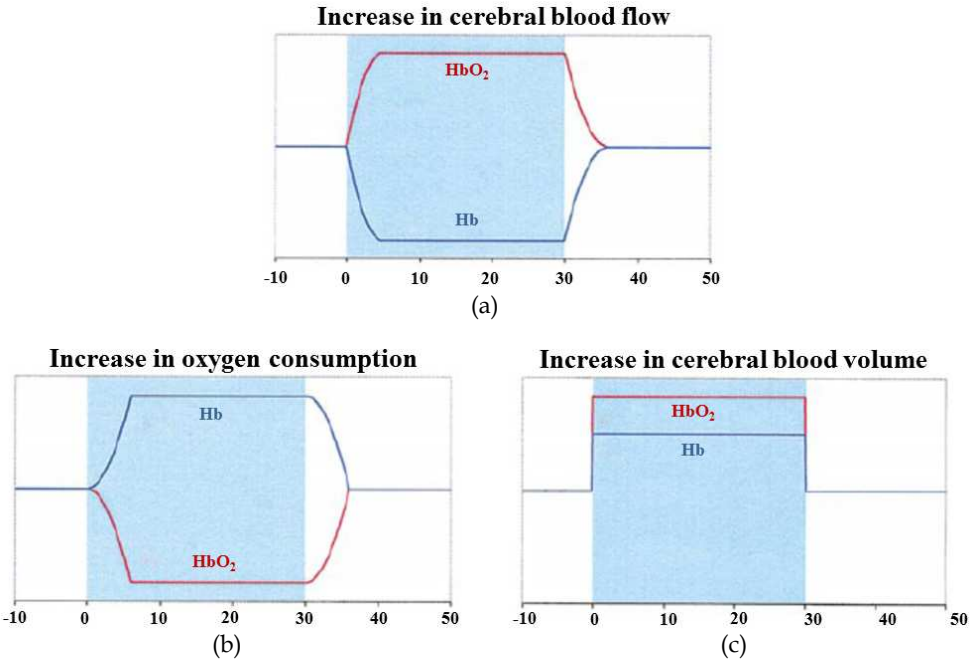

Fig. 9. The effect of an isolated increase in cerebral blood flow (a), cerebral metabolic rate of oxygen (b), or total hemoglobin concentration (c) on the time evolution of the [HbO_2] and [Hb] as predicted by the one-compartment model [Wolf et al., 2001].

adequate spatial resolution for continuously recording [HbO_2] and [Hb] changes of brain. Also, NIRS offers a more comprehensive measurement of brain activity than blood-oxygenation-level-dependent (BOLD) functional magnetic resonance imaging (fMRI).

Thus, NIRS can be used as a continuous monitor of changes in cerebral oxygenation and blood volume by following changes in the concentrations of [HbO_2] and [Hb]. It is also possible to make absolute measurements of CBF and CBV. NIRS has been applied to the measurement of tissue blood flow by using a small change in [HbO_2] as a tracer and applying a modification of the Fick principle which states that the amount of substance taken up by an organ per unit time is equivalent to the difference between the rate of the arrival of the substance, calculated as the product of blood flow through the organ by the arterial concentration of the substance, and the rate of the departure of the substance from the organ, calculated as the venous concentration of the substance. A small reduction in arterial saturation (of the order of 5%) is induced by lowering fractional inspired oxygen FiO_2. When a stable baseline is achieved, a breath of 100% oxygen creates a bolus of [HbO_2] in the arterial circulation which acts as the required Fick tracer. The rate of arrival of [HbO_2] in the brain a few seconds later can be observed by NIRS. CBF may be calculated by considering the ratio of the rate of tracer accumulation in the organ to the amount of tracer delivered. The accumulation of [HbO_2] in the brain is dependent on both arterial inflow and venous outflow.

The signal representing the difference between the change in [HbO_2] and [Hb] concentration, termed Δ HbD, is twice the amplitude of the signal corresponding to [HbO_2] change in concentration alone, therefore

$$CBF(ml.100^{-1}.min^{-1})=k_1 \cdot (\Delta HbD)/2 \cdot H \cdot \int 0 \to t \cdot \Delta SaO_2 \quad (16)$$

where K_1 is a constant reflecting the molecular weight of hemoglobin and cerebral tissue density; ΔSaO_2 is the change in arterial oxygen saturation by pulse oximetry; and H is the blood vessel hemoglobin concentration (g/dL). Application of this technique in the clinical field was demonstrated by Edwards and colleagues who showed that i.v. indomethacin administered to close a patent ductus arteriosus led to a marked decrease in CBF measured by NIRS.

Notwithstanding that CBF is the hemodynamic variable most familiar to clinicians, a combination of this information with other variables such as CBV would be valuable in interpreting changes in the clinical condition. Continuous measurement of changes in [tHb] generally reflects changes in CBV. Absolute quantification of CBV is also possible with NIRS. If arterial saturation is reduced by a small increment (approximately 5%) in a slow and controlled manner [HbO_2] is observed by NIRS to decline in parallel. As with CBF measurement, it is important that the change is small enough to avoid any effects on CBF or oxygen extraction. If arterial saturation is plotted against [HbO_2], the gradient of the resulting straight line is directly proportional to CBV. CBV can be calculated in absolute terms using a modification of a standard indicator dilution principle. Absolute CBV value can be derived from:

$$CBV(ml.100g^{-1})=k_2 \cdot (\Delta HbD)/2 \cdot H \cdot \Delta SaO_2 \quad (17)$$

where K_2 is obtained from K_1 and the large-vessel: tissue hematocrit ratio.

Consider a brain empty of blood. However much arterial saturation was varied, there could be no change in cerebral HbO_2 concentration and the gradient of the line would be zero. In contrast, a head with a high CBV would display a large change in $[HbO_2]$ for a small change in arterial saturation. As the units of the gradient are unfamiliar in the raw state it must be converted to CBV in the same way as described for tHb. This measurement can be used to provide a baseline value for CBV with which the real-time trends in [tHb] can be compared. Changes in cerebral intravascular oxygenation, equivalent to the difference between $[HbO_2]$ and [Hb], are an indicator of the mean oxygensaturation of hemoglobin in all types of blood vessels (arteries, capillaries and veins) in tissue. Thus, changes in cerebral blood volume can be assessed from changes in Δ [tHb], CBV can calculate by the proportionalities:

$$\Delta \text{ CBV}=k_2 \times \Delta \text{ [tHb]}/H \tag{18}$$

5.2 Near-infrared spectroscopy and imaging for breast cancer

NIRS has been used for clinical detection of various cancers, such as breast cancer, skin cancer, bladder cancer, lung cancer, brain tumors, and cervical cancer. For human breast imaging, NIRS reveals pathological tumor contrast directly in vascularity, hemoglobin concentration and tissue scattering property. Based on the modified Beer-Lambert's Law, the change of vascularity and oxygenation can be observed by utilizing optical measurements at multiple source-detector positions on the tissue surfaces. NIRS techniques use measurements of transmitted light to produce spatially resolved images. Images of the absorption or scattering properties of the tissue, or other physiological parameters such as tHb and StO_2 may be generated. Because the low spatial resolution in NIRS imaging technique, at present, the new diagnostic methods of NIRS imaging focusing on physiological properties detected of the breast tumor such as the hemoglobin response. In the case of human breast tissue, functional activation is not available and instead spatial differences must be employed. Localization and characterization of the incremental changes of optical properties with respect to position changes are necessary. Thus, the problem is significant and absolute values of optical properties involve problems of the physiological and biochemical baselines for distinguishing pathologies from normal and tumor region. The overall average tHb concentration and StO_2 for benign fibroadenoma and malignant lesions suggest that breast lesions contain at least twice the tHb concentration of healthy background breast tissue. This is supported by evidence suggesting that breast lesions have greater tHb concentrations compares to background tissues.

Some study provided specificity and sensitivity values to describe the ability of near-infrared imaging to detect malignancy based on spectroscopic information. One of study performed by Chance et al. was a 6 year, two site experiments that involved the use of a multi-wavelength handheld device, operating in CW domain. Data was acquired from 166 patients of whom 44 patients had confirmed malignancy and the remainder classified as non-cancer patients. Blood volume and saturations were calculated with reference to a similar location on the contralateral healthy breast. The results are summarized in the 2D normogram of blood volume and oxygen saturation in Fig. 10. The abscissa is relative increments of blood concentration in units of micro-molar concentration change with respect to the average cancer-free value. The ordinate represents incremental change with respect to the average cancer-free value in percent change of hemoglobin saturation. In this graph, verified cancers are indicated with a dot and cancer-free breasts plotted with an X. The normogram can be divided into two

zones, one containing the verified cancers (I) and the other containing cancer-free breasts (II). This technique was able to distinguish cancer from non-cancer bearing breasts with 96% sensitivity and 93% specificity, with an area under the curve of 95%.

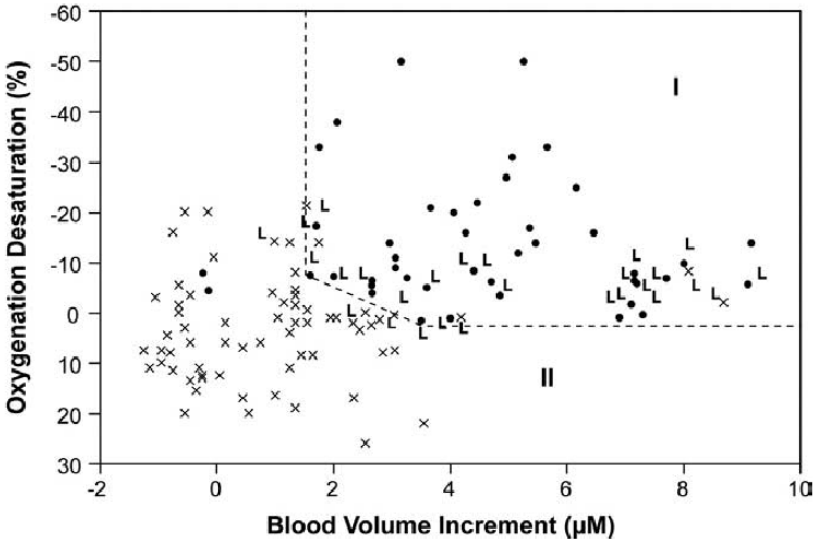

Fig. 10. A two-dimensional nomogram display of currently available NIR breast cancer data [Chance et al., 2005].

5.3 Intensive care unit

In intensive care medicine, real-time physiological monitoring of vital signs plays an important role in diagnosis and therapy, particularly for the cardiovascular assessment of patients with heart failure and/or sepsis. To maintain central blood pressure and vital organ perfusion, cardiovascular insufficiency may be overcome by increasing sympathetic output through the vasoconstriction of lesser vital organs and muscles. Unfortunately, this compensatory mechanism often masks profound hypovolemia. Currently, bedside assessment of cardiovascular adequacy involves either the measurement of the vital signs, blood lactate levels, and capillary refill, or the monitoring of tissue oxygenation using invasive techniques. The ability to characterize tissue oxygenation through non-invasive means would be of immense benefit in the intensive care unit (ICU). The approach of NIRS also can highly valuable for examining the effects of medication in the ICU.

Figure 11 (a) shows the group average response with a standard deviation of tHb and StO_2 for the VOT of normal subjects, respectively. Figure 11 (b) shows the tHb and StO_2 curves in response to the VOT in patients with heart failure. Obviously, the average response of tHb for patients with heart failure is lower and more slurred than that of normal subjects. A stepwise decreasing pattern in patients with heart failure characterized StO_2 tracing.

The NIRS is capable of accessing the spatial distribution of tissue oxygenation, and to do so in real-time. For qualitative comparisons, the greatest change in tissue oxygenation occurred at the beginning of VOT in healthy subjects, particularly with regard to changes in the

concentration of oxy-hemoglobin. Different temporal tracings reveal different physiological conditions. The temporal tracings of tissue oxygenation are measured using NIRS measurement and a VOT, employing normal subjects and ICU patients suffering from heart failure. The NIRS provides a highly potential on the oxygenation of muscles in the extremities measured during VOT in normal subjects and ICU patients.

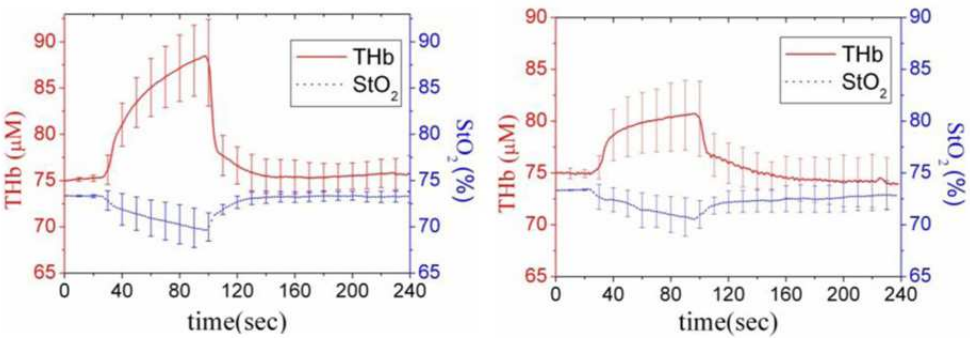

Fig. 11. Temporal tracings of the VOT response from normal control and heart failure patient tissue oxygen saturation (StO_2) and total hemoglobin (tHb) response [Wang et al., 2011].

5.4 The exercising test

NIRS is applied to study tissue oxygenation in skeletal muscle and brain under a variety of experimental conditions. The local hemoglobin status and blood flow is an important parameter for assessment of muscle physiology, particularly during exercise in both healthy and disease. The optical measurement of the near-infrared absorption coefficient at multiple wavelengths can be translated into measurements of the [HbO_2] and [Hb] in tissue. During exercise, both blood flow and oxidative metabolism in skeletal muscle respond to meet increased oxygen demand.

Figure 12 reports the results of an experiment to measure the desaturation in the legs of peripheral vascular disease (PVD) patients during stationary bicycle exercise. The comparison of the typical hemoglobin saturation traces recorded on healthy subject (blue line) and PVD patient (red line) in Fig. 12 shows the difference in the response of healthy and diseased legs. In the healthy subject, the hemoglobin saturation decreases slightly during the exercise, whereas the PVD patient shows a consistent decrease in hemoglobin saturation. The recovery time after exercise is also significantly shorter in the healthy subject than in the PVD patient. These results are consistent with an insufficient blood flow adjustment in the PVD patients to compensate for the increased oxygen demands during muscle exercise. The longer recovery time is also associated with the lower blood flow so that it requires more time to overcome the oxygen debt. In addition, the ability to characterize the muscular performance of athletes, during and after exercise leads to vital information in the field of sports medicine. These measurements may monitor the muscle tissue oxygenation and hemodynamics and assist in determining an athlete's exercise capacity, assessing the efficacy and validity of training programs and tracking an athlete's progress while in rehabilitative conditioning.

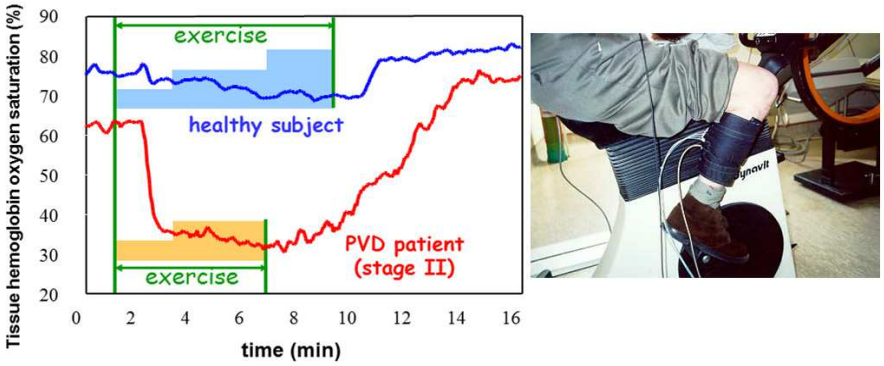

Fig. 12. Typical hemoglobin saturation traces of healthy and PVD patient [Sergio Fantini's Group, Department of Biomedical Engineering, Tufts University and in collaboration with R. Palumbo and G. Vaudo, Policlinico Monteluce, University of Perugia, Italy].

Knowledge of how the central nervous system (CNS) influences motor neurons to limit neuromuscular performance is nascent. It is accepted that motor command and its corollaries exist at multiple levels in the CNS to sustain homeostatic functions during exercise. Likewise, several metabolic and neurochemical pathways between skeletal

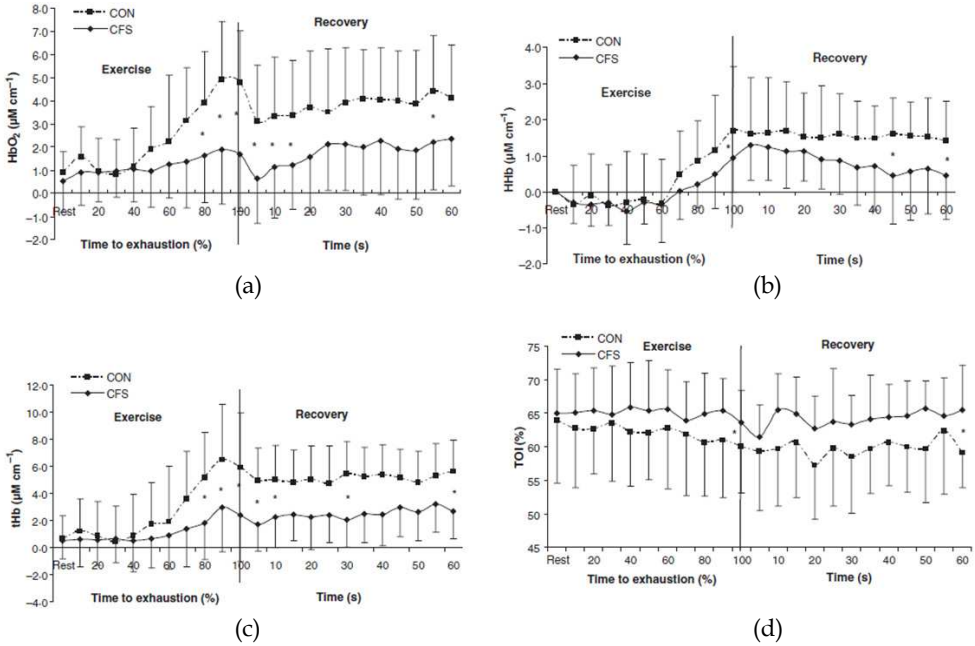

Fig. 13. Left prefrontal cortex (a) oxy-haemoglobin changes (HbO_2; lM cm); (b) deoxy-haemoglobin changes (HHb; lM cm); (c) total blood volume changes (tHb; lM cm) and (d) tissue oxygenation index (TOI %) in the chronic fatigue syndrome (CFS) and control (CON) subjects during continuous incremental maximal exercise and resting recovery [Neary et al., 2008].

muscles, the spinal cord, and the brain suggest ways by which exercise might influence the CNS. The studies of the brain during exercise have focused on cerebral hemodynamic responses. The use of NIRS to evaluate hemodynamic changes in the brain during exercise has increased as NIRS systems have become more available.

Figure 13 demonstrates the effects of maximal incremental exercise (performed an incremental cycle ergometer test to exhaustion) on cerebral oxygenation in chronic fatigue syndrome (CFS) and control (CON) subjects. Prefrontal cortex HbO_2, Hb and tHb were significantly lower at maximal exercise in CFS versus CON, as was TOI during exercise and recovery. The CFS subjects exhibited significant exercise intolerance and reduced prefrontal oxygenation and tHb response when compared with CON subjects. These data suggest that the altered cerebral oxygenation and blood volume may contribute to the reduced exercise load in CFS, and supports the contention that CFS, in part, is mediated centrally.

NIRS has been used as a practical indicator of cerebral oxygenation and hemodynamic change during sub-maximal and maximal exercise. As NIRS technology continues to improve, considerations of optode distance and location, and reconsideration of and use of quantifiable light signals will expand the information that can be obtained using NIRS during and after exercise to understand cortical brain function and its role in human performance and health, especially when NIRS is used with other neuroimaging measures concurrent with controlled manipulations of the brain.

5.5 Hemodialysis patients

Hemodialysis has direct and indirect effects on skin and muscle microcirculatory regulation that are severe enough to worsen tolerance to physical exercise and muscle asthenia in patients undergoing dialysis. Hemodialysis utilizes counter current flow, where the dialysate is flowing in the opposite direction to blood flow in the extracorporeal circuit. Several side effects, including low blood pressure, fatigue, chest pains, nausea, headaches and muscle-cramps, are originated by removing too much fluid rapidly. The patients on long-term hemodialysis suffer from a variety of syndrome problems, for example, muscle-cramps (ex: shoulder pain). Meanwhile, it leads to reduce oxygen concentration, especially with the ipsilateral of the arteriovenous fistula. NIRS has been shown to be an effective tool for measuring local changes of tissue in hemodynamics.

Diffuse optical imaging and spectroscopy with near-infrared light reconstructs tissue physiologic parameters based on noninvasive measurement of tissue optical properties. NIRS can provide a high potential to be extensively employed to evaluate human hemodynamics, and to widely use and explain in several clinical applications. The advantages brought by NIRS compared with the conventional techniques are numerous: it allows a non-invasive, real-time measurement of the concentrations of interest, the observation time is unlimited, it can be used to monitor the time evolution of the tissue oxygenation during physiological or metabolic processes, it uses instrumentation of relatively small dimensions and it is cost effective. All these characteristics are fundamental for clinical use. Furthermore, the optical method can provide completely "patient-oriented" measurement for clinical applications.

6. References

Ahmadi S., Sinclair P. J. and Davis G. M., Muscle oxygenation following concentric exercise, *Isokinet. Exerc. Sci.*, Vol. 15, pp. 309-319, 2007.

Blasi R. A. De, Palmisani S., Alampi D., Mercieri M., Romano R., Collini S. and Pinto G., Microvascular dysfunction and skeletal muscle oxygenation assessed by phase-modulation near-infrared spectroscopy in patients with septic shock, *Intensive Care Med.*, Vol. 31, pp. 1661-1668, 2005.

Beekvelt M. C. P. van, Engelen B. G. M. van, Wevers R. A. and Colier W. N. J. M., In vivo quantitative near-infrared spectroscopy in skeletal muscle during incremental isometric handgrip exercise, *Clin. Physiol. & Func. Im.*, Vol. 22, pp. 210-217, 2002.

Boas D. A., Gaudette T., Strangman G., Cheng X., Marota J. J. A. and Mandeville J. B., The accuracy of near-infrared spectroscopy and imaging during focal changes in cerebral hemodynamics, *NeuroImage*, Vol. 13, pp. 76-90, 2001.

Boushel R., Langberg H., Olesen J., Gonzales-Alonzo J., Bu¨low J. and Kjær M., Monitoring tissue oxygen availability with near infrared spectroscopy (NIRS) in health and disease, *Scand. J. Med. Sci. Sports*, Vol. 11, pp. 213-222, 2001.

Boushel R., Langberg H., Olesen J., Nowak M., Simonsen L., Bülow J. and Kjær M., Regional blood flow during exercise in humans measured by near-infrared spectroscopy and indocyanine green, *J. Appl. Physiol.*, Vol. 89, pp. 1868-1878, 2000.

Beekvelt M. C. P. Van, Colier W. N., Engelen B. G. M. van, Hopman M. T. E., Wevers R. A. and Oeseburg B., Validation of measurement protocols to assess oxygen consumption and blood flow in the human forearm by near infrared spectroscopy, *Proc. SPIE*, Vol. 3194, pp. 133-144, 1998.

Blasi R. A. De, Almenräder N., Aurisicchio P. and Ferrari M., Comparison of two methods of measuring forearm oxygen consumption (VO_2) by near-infrared spectroscopy, *J. Biomed. Opt.*, Vol. 2, pp. 171-175, 1997.

Belardinelli R., Barstow T. J., Porszasz J. and Wasserman K., Changes in skeletal muscle oxygenation during incremental exercise measured with near infrared spectroscopy, *Eur J. Appl. Physiol.*, Vol. 70, pp. 487-492, 1995.

Blasi R. A. De, Ferrari M., Natali A., Conti G., Mega A. and Gasparetto A., Noninvasive measurement of forearm blood flow and oxygen consumption by near-infrared spectroscopy, *J. Appl. Physiol.*, Vol. 76, pp. 1388-1393, 1994.

Chance B., Nioka S., Zhang J., Conant E. F., Hwang E., Briest S., Orel S. G., Schnall M. D. and Czerniecki B. J., Breast cancer detection based on incremental biochemical and physiological properties of breast cancers: A six-year, two-site study[1], *Acad. Radiol.*, Vol. 12, pp. 925-933, 2005.

Casavola C., Paunescu L. A., Fantini S. and Gratton E., Blood flow and oxygen consumption with near-infrared spectroscopy and venous occlusion: spatial maps and the effect of time and pressure of inflation, *J. Bio. Opt.*, Vol. 5, pp. 269-276, 2000.

Cubeddu R., Pifferi A., Taroni P., Torricelli A. and Valentini G., Noninvasive absorption and scattering spectroscopy of bulk diffusive media: An application to the optical characterization of human breast, *Applied Physics Letters*, Vol. 74, pp. 874-876, 1999.

Casavola C., Paunescu L. A., Fantini S., Franceschini M. A., Lugarà P. M. and Gratton E., Application of near-infrared tissue oxymetry to the diagnosis of peripheral vascular disease, *Clin. Hemorheol. Micro.*, Vol. 21, pp. 389-393, 1999.

Chance B., Optical method, *Annu. Rev. Biophys. Biophys. Chern.*, Vol. 20, pp. 1-28, 1991.

Dinh T. V., Biomedical photonics handbook, *Boca Raton London & New York*, 2003.

Edward A. D., Wyatt J. S., Richardson C., Potter A., Reynolds E. O. R., Cope M. and Delpy D. T., Effects of indomethacin on cerebral haemodynamics in very preterm infants, *The Lancet*, Vol. 335, pp. 1491-1495, 1990.

Fantini's S. Group, Optical study of muscle hemodynamics and oxygenation, Department of Biomedical Engineering, Tufts University. http://ase.tufts.edu/biomedical/research/fantini/research.asp

Hachiya T., Blaber A. P. and Saito M., Near-infrared spectroscopy provides an index of blood flow and vasoconstriction in calf skeletal muscle during lower body negative pressure, *Acta. Physiol.*, Vol. 193, pp. 117-127, 2008.

Homma S., Eda H., Ogasawara S. and Kagaya A., Near-infrared estimation of O2 supply and consumption in forearm muscles working at varying intensity, *J. Appl. Physiol.*, Vol. 80, pp. 1279-1284, 1996.

Jöbsis F. F., Noninvasive, infrared monitoring of cerebral and myocardial oxygen sufficiency and circulatory parameters, *Science*, Vol. 198, pp. 1264-1267, 1977.

Lai N., Zhou H., Saidel G. M., Wolf M., McCully K., Gladden L. B. and Cabrera M. E., Modeling oxygenation in venous blood and skeletal muscle in response to exercise using near-infrared spectroscopy, *J. Appl. Physiol.*,Vol. 106, pp. 1858-1874, 2009.

Leff D. R., Warren O. J., Enfield L. C., Gibson A., Athanasiou T., Patten D. K., Hebden J., Yang G. Z. and Darzi A., Diffuse optical imaging of the healthy and diseased breast: A systematic review, *Breast Cancer Res. Treat.*, Vol. 108, pp. 9-22, 2008.

Lin Y., Lech G., Nioka S., Intes X. and Chance B., Noninvasive, low-noise, fast imaging of blood volume and deoxygenation changes in muscles using light-emitting diode continuous-wave imager, *Rev. Sci. Instrum.*, Vol. 73, 3065-3074, 2002.

McCully K. K. and Hamaoka T., Near-Infrared Spectroscopy: What Can It Tell Us about Oxygen Saturation in Skeletal Muscle, *Exercise and sport sciences reviews*, Vol. 28, pp. 123-127, 2000.

Neary J. P., Roberts A. D. W., Leavins N., Harrison M. F., Croll J. C. and Sexsmith J. R., Prefrontal cortex oxygenation during incremental exercise in chronic fatigue syndrome, *Clin. Physiol. Funct. Imaging*, Vol. 28, pp. 364-372, 2008.

Nioka S., Kime R., Sunar U., Im J., Izzetoglu M., Zhang J., Alacam B. and Chance B., A novel method to measure regional muscle blood flow continuously using NIRS kinetics information, *Dynamic Medicine*, Vol. 5, pp. 1-13, 2006.

Pellicer A. and Bravo M. del C., Near-infrared spectroscopy: A methodology-focused review, *Semin. Fetal. Neonat. M.*, Vol. 16, pp. 42-49, 2011.

Prieur F., Berthoin S., Marles A., Blondel N. and Mucci P., Heterogeneity of muscle deoxygenation kinetics during two bouts of repeated heavy exercises, *Eur J. Appl. Physiol.*, Vol. 109, pp. 1047-1057, 2010.

Pogue B. W., Jiang S., Dehghani H., Kogel C., Soho S., Srinivasan S., Song X., Tosteson T. D., Poplack S. P. and Paulsen K. D., Characterization of hemoglobin, water, and NIR scattering in breast tissue: analysis of intersubject variability and menstrual cycle changes, *J. Bio. Opt.*, Vol. 9, pp. 541-552, 2004.

Prasad P. N., Introduction to biophotonics, *John Wiley & Sons Inc.*, 2003.

Quaresima V., Ferrari M., Franceschini M. A., Hoimes M. L. and Fantini S., Spatial distribution of vastus lateralis blood flow and oxyhemoglobin saturation measured at the end of isometric quadriceps contraction by multichannel near-infrared spectroscopy, *J. Bio. Opt.*, Vol. 9, pp. 413-420, 2004.

Quaresima V., Homma S., Azuma K., Shimizu S., Chiarotti F., Ferrari M. and Kagaya A., Calf and shin muscle oxygenation patterns and femoral artery blood flow during dynamic plantar flexion exercise in human, *Eur J. Appl. Physiol.*, Vol. 84, pp. 387-394, 2001.

Quaresima V., Franceschini M. –A., Fantini S., Gratton E. and Ferrari M., Difference in leg muscles oxygenation during treadmill exercise by a new near infrared frequency-domain oximeter, *Proc. SPIE*, Vol. 3194, pp. 116-120, 1998.

Sowa M. G., Leonardi L., Payette J. R., Fish J. S. and Mantsch H. H., Near infrared spectroscopic assessment of hemodynamic changes in the early post-burn period, *Burns*, Vol. 27, pp. 241-249, 2001.

Timinkul A., Kato M., Omori T., Deocaris C. C., Ito A., Kizuka T., Sakairi Y., Nishijima T., Asada T. and Soya H., Enhancing effect of cerebral blood volume by mild exercise in healthy young men: A near-infrared spectroscopy study, *Neurosci. Res.*, Vol. 61, pp. 242-248, 2008.

Tromberg B. J., Cerussi A., Shah N., Compton M., Durkin A., Hsiang D., Butler J. and Mehta R., Diffuse optics in breast cancer: detecting tumors in pre-menopausal women and monitoring neoadjuvant chemotherapy, *Breast Cancer Research*, Vol. 7, pp. 279-285, 2005.

Toronov V., Webb A., Choi J. H., Wolf M., Michalos A., Gratton E. and Hueber D., Investigation of human brain hemodynamics by simultaneous near-infrared spectroscopy and functional magnetic resonance imaging, *Med. Phys.*, Vol. 28, pp. 521-527, 2001.

Vo T. Van, Hammer P. E., Hoimes M. L., Nadgir S. and Fantini S., Mathematical model for the hemodynamic response to venous occlusion measured with near-infrared spectroscopy in the human forearm, *IEEE T. Bio-Med. Eng.*, Vol. 54, pp. 573-584, 2007.

Vernieri F., Tibuzzi F., Pasqualetti P., Rosato N., Passarelli F., Rossini P. M. and Silvestrini M., Transcranial doppler and near-infrared spectroscopy can evaluate the hemodynamic effect of carotid artery occlusion, *Stroke*, Vol. 35, pp. 64-70, 2004.

Villringer A., Planck J., Hock C., Schleinkofer L. and Dirnagl U., Near infrared spectroscopy (NIRS): a new tool to study hemodynamic changes during activation of brain function in human adults, *Neurosci. Lett.*, Vol. 154, pp. 101-104, 1993.

Wang C. -Y., Chuang M. -L., Liang S. -J., Tsai J. -C., Chuang C. -C., Hsieh Y. -S., Lu C. -W., Lee P. -L., and Sun C. -W., Diffuse Optical Multipatch Technique for Tissue Oxygenation Monitoring: Clinical Study in Intensive Care Unit, *IEEE T BIO-MED ENG.*, Vol. 59, pp. 87-94, 2011.

Wu Y. -T., Chiou A. and Sun C. -W., Correlation between tissue oxygenation and erythrocytes elasticity, *J. Biophotonics*, Vol. 4, pp. 224–228, 2011.

Wolf M., Wolf U., Toronov V., Michalos A., Paunescu L. A., Choi J. H. and Gratton E., Different time evolution of oxyhemoglobin and deoxyhemoglobin concentration changes in the visual and motor cortices during functional stimulation: A near-infrared spectroscopy study, *NeuroImage*, Vol. 16, pp. 704-712, 2002.

Yu G., Durduran T., Lech G., Zhou C., Chance B., Mohler III E. R. and Yodh A. G., Time-dependent blood flow and oxygenation in human skeletal muscles measured with noninvasive near-infrared diffuse optical spectroscopies, *J. Bio. Opt.*, Vol. 10, pp. 024027 1-12, 2005.

Zhang Z., Wang B., Gong H., Xu G., Nioka S. and Chance B., Comparisons of muscle oxygenation changes between arm and leg muscles during incremental rowing exercise with near-infrared spectroscopy, *J. Bio. Opt.*, Vol.15, pp. 017007 1-8, 2010.

Zhou C., Choe R., Shah N., Durduran T., Yu G., Durkin A., Hsiang D., Mehta R., Butler J., Cerussi A., Tromberg B. J. and Yodh A. G., Diffuse optical monitoring of blood flow and oxygenation in human breast cancer during early stages of neoadjuvant chemotherapy, *J. Biomed. Opt.*, Vol. 12, pp. 051903 1-11, 2007.

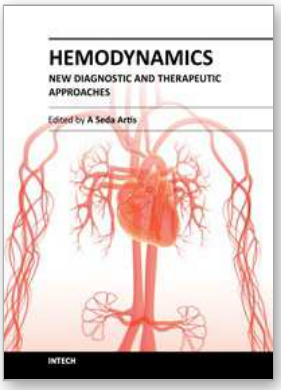

Hemodynamics - New Diagnostic and Therapeutic Approaches
Edited by Dr. A Seda Artis

ISBN 978-953-51-0559-6
Hard cover, 156 pages
Publisher InTech
Published online 25, April, 2012
Published in print edition April, 2012

Hemodynamics is study of the mechanical and physiologic properties controlling blood pressure and flow through the body. The factors influencing hemodynamics are complex and extensive. In addition to systemic hemodynamic alterations, microvascular alterations are frequently observed in critically ill patients. The book "Hemodynamics: New Diagnostic and Therapeuric Approaches" is formed to present the up-to-date research under the scope of hemodynamics by scientists from different backgrounds.

How to reference
In order to correctly reference this scholarly work, feel free to copy and paste the following:

Chia-Wei Sun and Ching-Cheng Chuang (2012). Hemodynamics Study Based on Near-Infrared Optical Assessment, Hemodynamics - New Diagnostic and Therapeutic Approaches, Dr. A Seda Artis (Ed.), ISBN: 978-953-51-0559-6, InTech, Available from: http://www.intechopen.com/books/hemodynamics-new-diagnostic-and-therapeutic-approaches/hemodynamics-study-based-on-near-infrared-optical-assessment

INTECH
open science | open minds

InTech Europe
University Campus STeP Ri
Slavka Krautzeka 83/A
51000 Rijeka, Croatia
Phone: +385 (51) 770 447
Fax: +385 (51) 686 166
www.intechopen.com

InTech China
Unit 405, Office Block, Hotel Equatorial Shanghai
No.65, Yan An Road (West), Shanghai, 200040, China
中国上海市延安西路65号上海国际贵都大饭店办公楼405单元
Phone: +86-21-62489820
Fax: +86-21-62489821